

# Journal of Materials Chemistry A

Accepted Manuscript



This is an *Accepted Manuscript*, which has been through the Royal Society of Chemistry peer review process and has been accepted for publication.

*Accepted Manuscripts* are published online shortly after acceptance, before technical editing, formatting and proof reading. Using this free service, authors can make their results available to the community, in citable form, before we publish the edited article. We will replace this *Accepted Manuscript* with the edited and formatted *Advance Article* as soon as it is available.

You can find more information about *Accepted Manuscripts* in the [Information for Authors](#).

Please note that technical editing may introduce minor changes to the text and/or graphics, which may alter content. The journal's standard [Terms & Conditions](#) and the [Ethical guidelines](#) still apply. In no event shall the Royal Society of Chemistry be held responsible for any errors or omissions in this *Accepted Manuscript* or any consequences arising from the use of any information it contains.



Journal

ARTICLE

## Improving the Stability and Selectivity for the Oxygen-Evolution Reaction on Semiconducting WO<sub>3</sub> Photoelectrodes with a Solid-State FeOOH Catalyst

Received 00th January 20xx,  
Accepted 00th January 20xx

DOI: 10.1039/x0xx00000x

www.rsc.org/

Charles R. Lhermitte,<sup>a</sup> J. Garret Verwer<sup>a</sup> and Bart M. Bartlett<sup>a\*</sup>

WO<sub>3</sub> electrodes were synthesized via a sol-gel route followed by the photoelectrochemical deposition of a solid state FeOOH oxygen-evolution catalyst (OEC) to observe its effects on electrode stability and selectivity towards the oxygen evolution reaction (OER). WO<sub>3</sub> photoanodes have been reported to degrade in aqueous solutions with pH > 3 due to the material's Arrhenius acidity and the potential formation of reactive peroxide intermediates on the WO<sub>3</sub> surface during the course of photoelectrochemical water oxidation. The stability during photoelectrochemical OER of WO<sub>3</sub> and WO<sub>3</sub>-FeOOH photoanodes was measured at 1.23 V vs. RHE at pH 4 and 7 in phosphate-buffered solutions. Additionally, the Faradaic efficiencies of the electrodes for OER were measured at pH 4. WO<sub>3</sub>-FeOOH electrodes demonstrate a 95.9 ± 1.6% Faradaic efficiency for OER in pH 4 potassium phosphate buffer at current densities of ~0.75 mA/cm<sup>2</sup> under 200 mW/cm<sup>2</sup> AM1.5G illumination and an applied bias of 1.43 V vs. RHE. These experiments demonstrate that adding an FeOOH co-catalyst dramatically improves the stability of the electrodes versus that observed on WO<sub>3</sub> films.

### Introduction

Developing a water splitting photoelectrochemical (PEC) cell with high efficiency for solar-to-hydrogen fuel conversion remains a challenge due to the rate-limiting oxygen evolution reaction (OER). Because this step involves the coupled transfer of 4 electrons and 4 protons, it is much slower than the hydrogen evolution reaction (HER). As a result, a large body of research has been dedicated to improving the rate of this reaction.<sup>1-11</sup>

WO<sub>3</sub> is an attractive candidate for use as a photoanode due to its ability to absorb visible ( $E_g = 2.7\text{eV}$ ) light and its possession of a valence band edge that is suitable for water oxidation.<sup>1-6</sup> It is predicted to be thermodynamically stable when used as a photoanode for water oxidation (OER) due to its anodic decomposition potential being located 1.1 V more positive than the OER potential.<sup>7</sup> However, it has been observed that WO<sub>3</sub> gradually loses its catalytic performance over time when used in this configuration. This effect is further exacerbated at higher pH values. The source of this degradation is two-fold; first WO<sub>3</sub> can behave as an Arrhenius acid, which reduces its stability in more basic solutions since it has the potential to undergo acid-base reactions with OH<sup>-</sup> in solution.<sup>8,9,10</sup> Additionally, it is known that during the course of PEC OER, WO<sub>3</sub> produces and accumulates peroxo- species on

its surface, which can accelerate its degradation.<sup>7,11</sup> These two effects are suspected to be the cause of the decrease in stability and Faradaic efficiency for OER on WO<sub>3</sub> at pH increases. A potential solution to stabilize the surface of WO<sub>3</sub> would be to grow an oxygen evolution (OEC) catalyst on the surface. This strategy has been previously demonstrated to work with cobalt phosphate (CoPi) and nickel borate (NiBi) OECs on WO<sub>3</sub> and BiVO<sub>4</sub> photoanodes.<sup>7,12</sup> Recently, it has been shown that electrochemically grown NiOOH and FeOOH films can function effectively as catalysts for OER.<sup>13-18</sup> However, the coupling of these particular OECs to the surface of a light-absorbing metal oxide has been limited to BiVO<sub>4</sub> and Fe<sub>2</sub>O<sub>3</sub>.<sup>12,19,20</sup> Ni and Fe based oxyhydroxides are ideal candidates for use as co-catalysts on WO<sub>3</sub> due to the simplicity of their syntheses and the earth abundance of their constituent elements. To date, there have been no reports of coupling FeOOH with WO<sub>3</sub>, and we hypothesize that FeOOH is particular is well suited to function in tandem with WO<sub>3</sub> during PEC OER since it can be easily deposited from an acidic solution, thereby circumventing the issue of degrading the WO<sub>3</sub> during the deposition process. In this report, we synthesized WO<sub>3</sub> via a simple sol-gel method and photoelectrochemically deposited an FeOOH OEC on its surface. Indeed, we demonstrate that adding the FeOOH OEC on WO<sub>3</sub> leads to increased stability and Faradaic efficiency for OER.

### Experimental

<sup>a</sup> Department of Chemistry, University of Michigan, 930 N. University Avenue, Ann Arbor, Mi 48109-1055, United States

Electronic Supplementary Information (ESI) available: [details of any supplementary information available should be included here]. See DOI: 10.1039/x0xx00000x

**Materials.** Hydrochloric acid (HCl, 36.5-38%) was purchased from VWR. Sodium tungstate ( $\text{NaWO}_4$ , 99+% ACROS Organics), potassium hydrogen phosphate ( $\text{K}_2\text{HPO}_4$ , 98.0% min., Alfa Aesar), potassium dihydrogen phosphate ( $\text{KH}_2\text{PO}_4$ , 99.0% min., Alfa Aesar), potassium hydroxide (KOH pellets,  $\geq 85.0\%$ , Fisher Chemical) and iron (II) chloride (Alfa Aesar, 99.5%) were purchased from Fisher Scientific. The authors would like to note that they tried using  $\text{FeCl}_2$  from other vendors, however the solubility was different possibly due to impurities present, so only  $\text{FeCl}_2$  from Alfa Aesar was used in these experiments. All reagents were used as purchased without further purification. Solutions were prepared using high purity water (Millipore Milli-Q purification system, resistivity  $> 18.2 \text{ M}\Omega$ ).

**Synthesis of  $\text{WO}_3$  Electrodes.** The  $\text{WO}_3$  electrodes used in this work were prepared via a sol-gel method adapted from a previous report.<sup>11,21,22</sup> 10 mmol (3.29 g) of sodium tungstate dihydrate was dissolved in 20 mL deionized water and run through a Dowex ion exchange column that had been acidified previously with 6 M HCl and rinsed back to pH 7 with Milli-Q water. A yellow solution was eluted into in a round-bottom flask containing 20 mL absolute ethanol while stirring. The resulting transparent yellow solution (tungstic acid) was concentrated on a rotovap until the final volume was approximately 20 mL, at which time 6.6 g PEG-300 (TCI, lot. UP2XKAA, d 1.13) was added as a stabilizer. At this point, the solution was significantly more viscous and had a cloudy yellowish color. The suspension was kept stirring constantly at 1200 rpm on a stir plate and used for up to 3 days. Over time the solution's color turned dark green. However, this color change did not appear to affect the consistency or quality of the resulting electrodes.  $\text{WO}_3$  electrodes were synthesized by dropping 30  $\mu\text{L}$  of the suspension onto clean FTO slides (Pilkington Glass, TEC-15) and spinning at 2500 rpm using a Laurel spin coater for 30 seconds, followed by annealing the electrodes in a muffle furnace preheated to  $500^\circ\text{C}$  for 30 minutes in air. The electrode area was kept at  $1 \text{ cm}^2$  by masking off the electrode with electrical tape prior to spin coating. The spinning and annealing process was repeated ten times to obtain electrodes of sufficient thickness (ca.  $2 \mu\text{m}$ ).

**Growth of FeOOH Films.** A FeOOH co-catalyst layer was grown using a PEC deposition onto the  $\text{WO}_3$  by applying a bias of 0.4 V vs. Ag/AgCl while front illuminating a  $1 \text{ cm}^2$   $\text{WO}_3$  electrode with  $100 \text{ mW}/\text{cm}^2$  of AM1.5G light in a 0.1 M solution of  $\text{FeCl}_2$  in Millipore water (pH  $\sim 4$ ). The PEC deposition was stopped after 0.087 C of charge had passed, which took approximately 5 – 10 minutes. The purpose of the PEC deposition step is to generate nucleation sites for the FeOOH near the areas with the highest concentration of photogenerated electron-hole pairs. Following the PEC deposition, an electrochemical (EC) deposition was performed by applying a bias of 1.2 V vs. Ag/AgCl in the dark in the same  $\text{FeCl}_2$  solution. This deposition was performed until 0.07 C of charge had passed, which also took 5 – 10 minutes.

**Materials Characterization.** X-ray diffraction was recorded on a Bruker D8 Advance diffractometer equipped with a graphite monochromator, a Lynx-Eye detector, and parallel beam optics using Cu  $K\alpha$  radiation ( $\lambda = 1.54184 \text{ \AA}$ ). Patterns were collected

using a 0.6 mm incidence slit, with a step size and scan rate of  $0.04^\circ/\text{step}$  and  $0.5 \text{ s}/\text{step}$ , respectively. The  $\text{WO}_3$  phase was identified as  $\text{WO}_3$  (JCPDF 72-0677) using MDI Jade version 5.0.

UV-vis spectra were recorded using a Cary 5000 spectrophotometer (Agilent) equipped with an external diffuse reflectance accessory. Spectra were recorded in reflectance mode and transformed mathematically into the Kubelka-Munk function,  $F(R)$ .

Scanning electron microscopy (SEM) images were collected using an FEI Nova Nanolab SEM/focused ion beam (FIB) instrument with an accelerating voltage of 10 kV, WD of 5 mm and beam current of 0.54 nA. For cross-sectional images, the  $\text{WO}_3/\text{WO}_3\text{-FeOOH}$  electrodes were sputter coated with Au for 10 s to dissipate surface charging and ease the imaging process.

**Photoelectrochemistry.** Photoelectrochemistry was performed using a CH Instruments 760 E electrochemical workstation. All PEC measurements were performed in custom-built cells with quartz viewing windows. Three-electrode voltammetry experiments were performed using the working  $\text{WO}_3/\text{WO}_3\text{-FeOOH}$  thin-film photoanode, a Ag/AgCl (saturated KCl) reference electrode, and a Pt wire counter electrode. The supporting electrolyte in all PEC experiments was 0.1 M  $\text{KPi}$  at pH 4 or 7. Unless specified otherwise, a  $1 \text{ cm}^2$  area of the working electrode from the back side (glass side) was irradiated through a quartz window. Freshly prepared electrodes were employed to start each experiment to avoid cracking of the FeOOH by dehydration of the film. The light source was a Newport-Oriel 150W Xe arc lamp fitted with an AM1.5G simulating solar filter (Newport). The lamp power was adjusted to  $100 \text{ mW}/\text{cm}^2$  (except for  $\text{O}_2$  detection experiments described below) using an optical power meter (Newport 1918-R) equipped with a thermopile detector (Newport 818P-015-19).

**Oxygen-Evolution Measurements.** Oxygen detection was performed in a custom-built two-compartment cell separated by a fine frit. For  $\text{O}_2$  detection experiments, the working electrode, Ag/AgCl reference electrode, and fluorescence probe (FOSSPOR, 1/8 in., Ocean Optics Inc.) were sealed in one compartment, separated from the Pt auxiliary electrode. To generate significant quantities of  $\text{O}_2$  to provide a good signal, the  $\text{O}_2$  detection experiments were carried out at 1.43 V vs RHE in 0.1 M  $\text{KPi}$  electrolyte using an AM1.5G filter and custom-built water filter. The lamp power was adjusted to  $200 \text{ mW}/\text{cm}^2$ . The number of moles of  $\text{O}_2$  produced was determined from the ideal gas law using the measured volume of the head space, the temperature recorded using a NeoFox temperature probe, and the partial pressure of  $\text{O}_2$  recorded by the FOSSPOR fluorescence probe. Dissolved  $\text{O}_2$  in the solution was accounted for through Henry's law using the measured partial pressure of  $\text{O}_2$  and the volume of solution in the cell. Throughout the experiment, the solution was stirred to aid  $\text{O}_2$  dissociation from the working electrode. The working electrode compartment contained 20 mL of electrolyte and 25 mL of head space. The fluorescence probe was calibrated with a two point calibration (0.00%  $\text{O}_2$  and 20.9%  $\text{O}_2$ ) using NeoFox software (Ocean Optics Inc.). Before the experiment was

begun, the percentage of O<sub>2</sub> was recorded for 30 – 45 min to ensure the cell was sealed completely from the atmosphere and to create a baseline. Then, it was measured for a period of time after the light was turned off. An important note is that during O<sub>2</sub> measurements, some O<sub>2</sub> was detected that was not produced photoelectro-chemically, but was detected because of drift in the fluorescence probe's calibration as the temperature slightly increased over the course of illumination. This fluctuation was accounted for by subtracting it from the baseline in the data work up. The Faradic efficiency was determined by dividing the measured moles of O<sub>2</sub> by the theoretical yield, which is determined by dividing the total charge passed during the experiment by 4*F* (4-electron oxidation, *F* = Faraday's constant, 96 485 C/mol of e<sup>-</sup>).

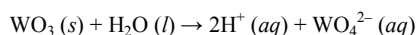
**External Quantum Efficiency Measurements.** Quantum efficiency measurements were obtained with an Oriel 150 W Xe arc lamp (Newport) and a quarter-turn single-grating monochromator (Newport). Sample measurements were recorded with chopped illumination (15/20 Hz), and a quartz beam splitter was used to simultaneously record the light output intensity with a separate Si photodiode (Newport) to adjust for fluctuations in lamp intensity. The potential of the working photoelectrode was poised to 1.23 V vs. RHE, and the absolute photocurrent was measured by a digital PAR 263 potentiostat. The output current signal was connected to a Stanford Instruments SR830 lock-in amplifier, and the output signals from the lock-in amplifier and the reference Si photodiode were fed into a computer controlled by custom-written LabVIEW software. Spectral response measurements were obtained in a pH 4 0.1 M KP<sub>i</sub> buffered solution.

## Results

WO<sub>3</sub> electrodes were synthesized via a sol-gel method. By spin coating a tungstic acid colloid that was produced by running a sodium tungstate solution through an ion exchange column and repeatedly annealing at 500°C after each layer, WO<sub>3</sub> electrodes with a glassy greenish appearance were obtained. XRD data (Fig. S1, ESI) reveal that the films are phase pure monoclinic WO<sub>3</sub> and SEM images (Fig. 1) show that the films appear to be dense and homogeneous in texture. The cross-sectional SEM image indicate that the films are ~2 μm thick

and comprised of interconnected nanoparticles with some porosity.

WO<sub>3</sub> is known to display poor stability in higher pH aqueous solutions.<sup>8</sup> To gain more insight concerning the degradation of the WO<sub>3</sub> electrodes, representative samples were left to soak overnight without stirring in pH 4 and pH 7 KP<sub>i</sub> solutions. After the overnight soak, the morphology of the electrode left in the pH 4 solution appeared unchanged via SEM. On the other hand, there was a visible amount of WO<sub>3</sub> removed from the electrode soaked in the pH 7 solution. These SEM images (Fig. 2) reveal that the WO<sub>3</sub> soaked in the pH 7 solution had eroded significantly, most likely due to aqueous acid-base reaction<sup>8</sup>:



As for the electrode soaked in the pH 4 solution, the material does not appear to have degraded significantly via SEM imaging. Furthermore, chopped light linear sweep voltammograms (CL-LSVs) of the two films were collected in pH 4 KP<sub>i</sub> before and after soaking the films overnight in their respective solutions (Fig. S2, ESI). The WO<sub>3</sub> electrode soaked in the pH 7 KP<sub>i</sub> demonstrate a 95% (0.038 mA/cm<sup>2</sup> vs 0.808 mA/cm<sup>2</sup>) loss in saturated photocurrent. On the other hand, the electrode soaked in the pH 4 KP<sub>i</sub> electrode surprisingly displays a 9.7% (0.947 mA/cm<sup>2</sup> vs. 0.863 mA/cm<sup>2</sup>) increase in saturated photocurrent. The observed increase may simply be due to the overnight soaking acting as a pre-treatment which may render the WO<sub>3</sub> surface more catalytically active. This is supported by the concurrent increase in electrocatalytic current in the CL-LSV. The importance of pre-treatments in increasing catalytic activity has been previously reported with other materials.<sup>15,16,23</sup> These results indicate that acid base interactions in the 0.1 M pH 4 KP<sub>i</sub> solution may not be the primary cause for the observed degradation in photocurrent during controlled potential coulometry (CPC or bulk electrolysis).

To improve the stability and Faradaic efficiency for OER of the sol-gel WO<sub>3</sub> photoanode, a solid state FeOOH electrocatalyst was deposited on its surface. The growth of the FeOOH film was accomplished by combining a photoelectrochemical (PEC) deposition followed by an electrochemical (EC) deposition in a 0.1 M FeCl<sub>2</sub> solution. This

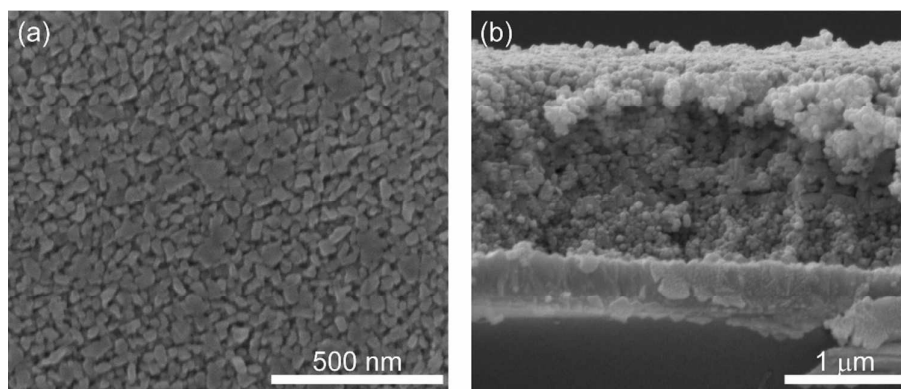


Fig. 1. a) Top-down SEM image of a WO<sub>3</sub> photoanode, b) cross-section of a WO<sub>3</sub> photoanode.

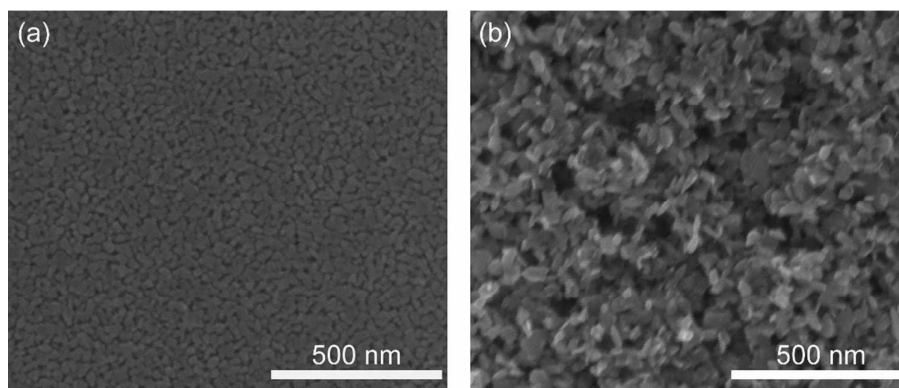


Fig. 2: SEM images of  $\text{WO}_3$  electrodes soaked in a) pH 4 and b) pH 7 KPI buffered solutions overnight.

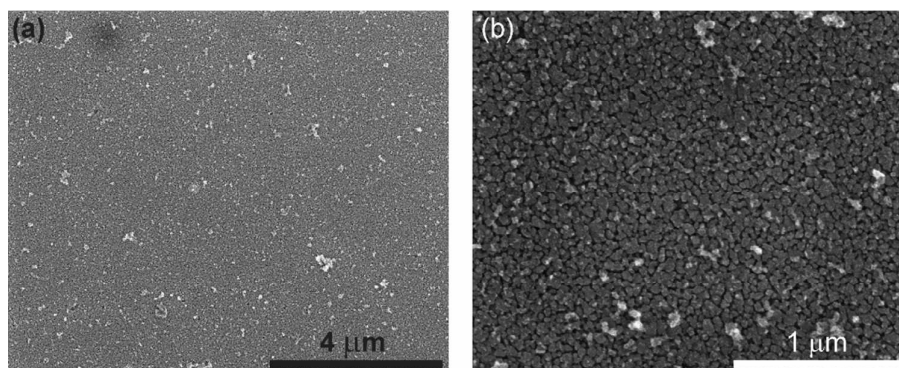


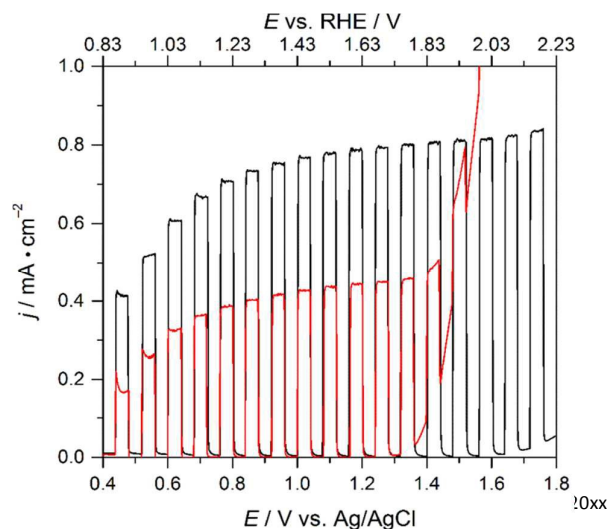
Fig. 3: SEM images of  $\text{WO}_3$ -FeOOH at a) 25K magnification and b) 100K magnification.

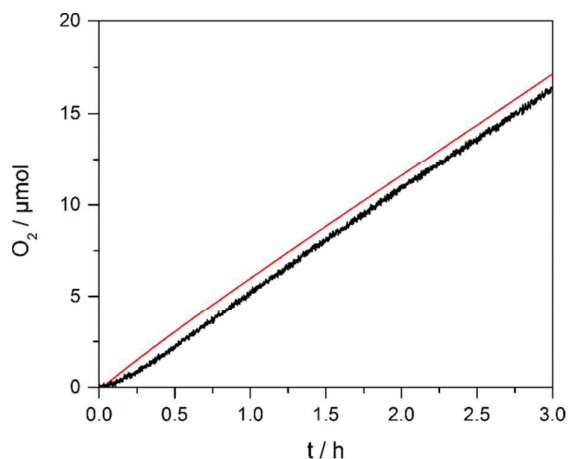
procedure was adapted from one previously published to deposit FeOOH onto  $\text{BiVO}_4$ .<sup>12</sup> It was observed that preceding an EC step with a short PEC deposition appeared to increase the rate of film growth for the EC deposition that followed. Thus it was hypothesized that the PEC deposition served to generate nucleation sites nearest to where the electron-hole pairs are generated under illumination, which would then allow more rapid film growth during the EC deposition step. Unless specified otherwise, after the FeOOH film was grown, the electrodes were immediately used (within minutes) in the following experiments. This prevented cracks from forming due to dehydration of the electrode (Fig. S3 ESI).

After FeOOH deposition, the morphology of the resulting films do not appear significantly altered via SEM imaging (Fig 3). Rather, small islands of FeOOH form on the surface of the  $\text{WO}_3$ . It must be noted that the  $\text{WO}_3$  films appear somewhat porous, so it is possible that there may be FeOOH deposited in the interstices of the film, which may not be easily viewed via SEM. The FeOOH itself appears to be amorphous, displaying no distinct Bragg reflections in its XRD pattern (Fig. S4, ESI). Nevertheless, the presence of Fe on the surface of the  $\text{WO}_3$  was confirmed via EDX spectroscopy (Fig. S5, ESI). In addition, the onset of electrocatalytic current in CL-LSVs shifts to much lower overpotentials, indicating the presence of the OEC on the  $\text{WO}_3$  surface (Fig. 4).

We note that the growth of FeOOH on  $\text{WO}_3$  decreases the saturated photocurrent by 48 – 50%, from  $\sim 0.8$  to  $\sim 0.4$   $\text{mA}/\text{cm}^2$  for an average film (Fig. 4). However, because the measured current density is a sum of all current derived from

the electrochemical reactions occurring at the surface, this means that not all the current generated is from the desired OER in the case of the bare  $\text{WO}_3$  electrodes. We note that another possible cause of the decrease in measured photocurrent density may be due to competitive light absorption from the FeOOH. The UV-vis absorption spectra (*vide infra*, Fig. S6, ESI) indicate that the FeOOH does indeed absorb visible light ( $\lambda_{\text{max}}$  of 425 nm), so it may compete with  $\text{WO}_3$  for light absorption. Furthermore, CL-LSVs with FeOOH grown on FTO (Fig. S7, ESI) demonstrate that any light absorbed by the FeOOH does not contribute to the photoresponse of the  $\text{WO}_3$ -FeOOH system, thus any current generated is solely due to electron-hole pairs generated within the  $\text{WO}_3$ . To evaluate better how competitive absorption from the FeOOH layer might affect electrode behavior, CL-LSVs with





front (electrode /electrolyte) and back (substrate/electrode)

**Fig. 4:** Chopped Light linear sweep voltammograms (CL-LSVs) of a  $\text{WO}_3$  electrode before (black) and after the growth of an FeOOH OEC (red) in pH 4 KPi buffered solution under 1 sun AM1.5G illumination

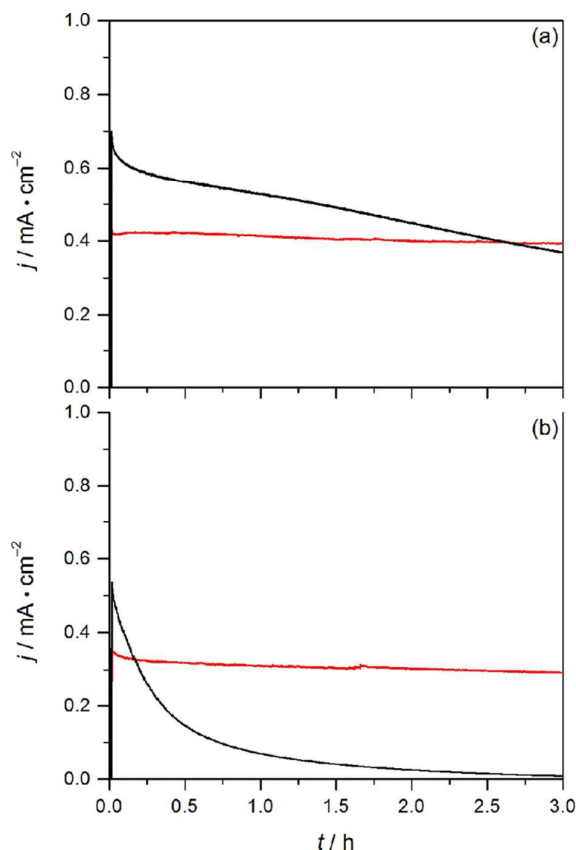
**Fig. 5:** Faradaic Efficiency of  $\text{WO}_3$ -FeOOH (1.43 V vs. RHE, pH 4 0.1 M KPi, 200mW/cm<sup>2</sup> AM1.5G illumination). Red line represents theoretical amount of  $\text{O}_2$  produced calculated from the charge passed during the experiment. The black line indicates the  $\text{O}_2$  measured using a fluorescence probe. The Faradaic efficiency measured in this case was 95.6%.

illumination were collected (Fig. S8, ESI). Upon front-side illumination, the  $\text{WO}_3$ -FeOOH electrode displays saturated photocurrent densities of 0.35 mA/cm<sup>2</sup>. However, upon back-side illumination, the current does indeed increase by 71% or from 0.35 to 0.6 mA/cm<sup>2</sup>. Although an increase in the saturated current density is observed upon back illumination, it is still possible that the FeOOH functions as a co-incorporated layer, and thus still provides parasitic absorption. In order to reduce this effect, all PEC experiments reported herein are conducted with back illumination unless specified otherwise.

The Faradaic efficiency for OER on the FTO| $\text{WO}_3$ |FeOOH hybrid electrodes (hereafter denoted as  $\text{WO}_3$ -FeOOH) was evaluated by measuring the  $\text{O}_2$  produced with a commercial fluorescence probe during a CPC experiment. These  $\text{O}_2$ -probe measurements were conducted under 200 mW/cm<sup>2</sup> AM1.5G illumination (2-suns) at 1.43 V vs. RHE in a pH 4 KPi solution in order to generate enough  $\text{O}_2$  to obtain sufficient accuracy. To determine the maximum quantity of  $\text{O}_2$  that could be generated from water photoelectrochemically, the charge passed after 3.5 hours was converted to  $\mu\text{mol}$   $\text{O}_2$  using the following equation:

$$O_2 (\mu\text{mol}) = \frac{\text{Charge Passed (C)} \times 10^6 \left( \frac{\mu\text{mol } O_2}{\text{mol } O_2} \right)}{4 \left( \frac{\text{mol } e^-}{\text{mol } O_2} \right) \times 96485 \left( \frac{\text{C}}{\text{mol } e^-} \right)}$$

The Faradaic efficiency is then computed by dividing the  $\text{O}_2$  measured after 3.5 hours by the maximum possible quantity of  $\text{O}_2$  then multiplying by 100. The  $\text{O}_2$  measured after 3.5 hours was used to calculate the Faradaic efficiency because we note that large amounts of bubbles stick to the reference electrode



and the sides of the cell after the lamp was turned off even with vigorous stirring, which causes the  $\text{O}_2$  signal to continue rising as  $\text{O}_2$  was being driven off. The signal typically stabilizes within 30 minutes of the light being turned off. The Faradaic efficiency for OER on  $\text{WO}_3$ -FeOOH hybrid electrodes is  $95.9 \pm 1.6\%$ , averaged over three trials. Fig. 5 depicts a representative Faradaic efficiency measurement for a  $\text{WO}_3$ -FeOOH electrode in

**Figure 6:** CPC curves of  $\text{WO}_3$  (black) and  $\text{WO}_3$ -FeOOH (red) at 1.23V vs. RHE and 1-sun illumination in a) pH 4 and b) pH 7 0.1M KPi solutions.

a 0.1 M pH 4 KPi solution, with full data for the three trials provided as Fig. S9, ESI. In contrast, the bare  $\text{WO}_3$  electrodes demonstrated an average Faradaic efficiency for OER of  $26.8 \pm 3.2\%$  over three trials (Fig. S10, ESI) which agrees well with previously published work.<sup>24</sup> Thus the  $\text{WO}_3$ -FeOOH electrodes display an increase of  $\sim 70\%$  in Faradaic Efficiency for OER over bare  $\text{WO}_3$ .

In addition to the Faradaic efficiency, we evaluated the stability of the hybrid electrode in aqueous KPi solutions. For these experiments, CPC at 1.23 V vs. RHE under 1-sun illumination was conducted for 3 hours in pH 4 and in pH 7 KPi buffered solutions (Fig. 6). In the pH 4 solution, the  $\text{WO}_3$  electrode gradually produces less photocurrent, decaying from 0.70 to 0.37 mA/cm<sup>2</sup>, indicating that the electrode is undergoing photodegradation. On the other hand, the  $\text{WO}_3$ -FeOOH electrode displays a stable photoelectrolysis curve over the three hours with its final current of 0.39 mA/cm<sup>2</sup> surpassing that of  $\text{WO}_3$ . Additionally, when the pH of the

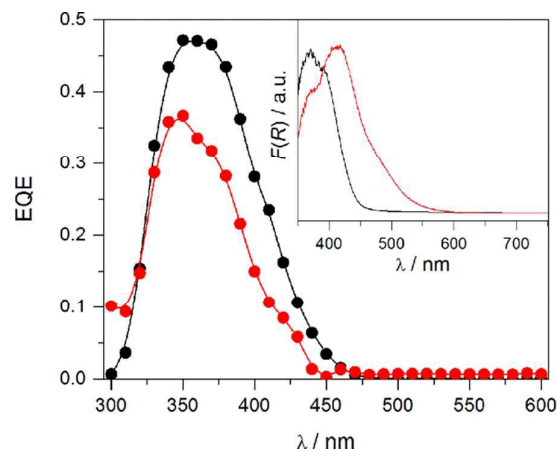
solution is increased to 7, the  $\text{WO}_3$  electrode undergoes rapid degradation in which it loses  $\sim 70\%$  of its photocurrent in 30 minutes. However, the  $\text{WO}_3\text{-FeOOH}$  electrode displays a much more stable electrolysis curve during that time period, losing less than 20% of the initial current density (from 0.35 to 0.29  $\text{mA}/\text{cm}^2$ ). Finally, by the end of the experiment, the control film was completely removed from the surface of the electrode while the  $\text{WO}_3\text{-FeOOH}$  electrode appeared unchanged.

**Fig. 7:** EQE of  $\text{WO}_3$  (black) and  $\text{WO}_3\text{-FeOOH}$  (red) at 1.23V vs. RHE in a 0.1M pH 4 KPi buffered solution with a light chopping frequency of 20 Hz. Inset: absorption spectrum of a  $\text{WO}_3$  film before (black) and after (red) growing an FeOOH catalyst on the surface.

Furthermore, the chemical stability of  $\text{WO}_3\text{-FeOOH}$  electrodes was probed by soaking them in aqueous KPi solutions at pH 4 and 7 overnight. CL-LSVs collected in pH 4 buffer both before and after the soaking (Fig. S11, ESI) indicate that no chemical degradation occurred in either pH, and thus the FeOOH is able to function as a true protective layer. This behavior is in stark contrast to control  $\text{WO}_3$  electrodes which degraded significantly—losing as much as 90% of the photocurrent after having been soaked in a pH 7 KPi solution overnight.

The external quantum efficiencies (EQE) and UV-Vis spectra for  $\text{WO}_3$  and  $\text{WO}_3\text{-FeOOH}$  electrodes are compared in Fig. 7. When back illuminated, the  $\text{WO}_3$  electrodes display EQE values of 45 – 47% in the wavelength range 350 – 400 nm. Toward longer wavelengths, the EQE decreases, which is reflective of  $\text{WO}_3$ 's indirect band gap ( $E_g = 2.7$  eV or 459 nm). Once the FeOOH is added, the EQE decreases by about 10% in the region of 350 – 400 nm. The source of this may be threefold. First, the growth of the OEC layer on top of the  $\text{WO}_3$  introduces a new heterojunction that could behave as a recombination center for electrons and holes.<sup>25</sup> Secondly, it is known that  $\text{WO}_3$  displays relatively low Faradaic efficiency for OER and thus it will readily oxidize other species in solution.<sup>24,26,27</sup> Thus, adding a selective OEC layer on the surface will block these side reactions from occurring, which could account for the lower measured current. Finally, the FeOOH may be behaving as a competitive light absorber, which would reduce the amount of photons reaching the  $\text{WO}_3$ .

Additionally, the possibility of transient incorporation into the EQE data was examined since this transient photocurrent can lead to inflated values. For this experiment, the EQE of a single  $\text{WO}_3$  film was measured at 15 and 20 Hz light chopping frequencies before and after loading the FeOOH (Fig. S12 ESI). We observed an increase in EQE with decreasing chopping frequency for both the  $\text{WO}_3$  and the  $\text{WO}_3\text{-FeOOH}$  case. This result indicates that transient incorporation into the data at 20 Hz is not significant. Furthermore, we attribute the observed increase in EQE with decreasing chopping frequency to a slow photocurrent response time of the electrode either due to slow kinetics for OER on the surface (*i.e.* the time constant for the reaction is longer than the chopping frequency), or due to slow carrier mobility within the electrode. This type of behavior has been observed in similar systems such as DSSCs



which also rely on a chemical redox event to supply current.<sup>28</sup> However, at both chopping frequencies, a decrease in EQE was still observed upon the growth of the FeOOH, which further supports the notion that FeOOH may be competitively absorbing light.

## Discussion

As an electrocatalyst, FeOOH is known to evolve oxygen from water at moderate overpotentials of  $\sim 300$  mV, but it has not been investigated as thoroughly as its Co and Ni counterparts.<sup>29,30</sup> Furthermore, examples of coupling the FeOOH OEC with a semiconducting metal oxide light absorber are limited, and only one such case using  $\text{BiVO}_4$  has been reported so far.<sup>12</sup> Thus, we desired to measure how the growth of this co-catalyst influences electrode stability and Faradaic efficiency for OER. We hypothesized that by depositing the FeOOH oxygen evolution catalyst on the surface of  $\text{WO}_3$ , we would shift the OER to FeOOH sites rather than  $\text{WO}_3$  sites, which in turn, would protect the  $\text{WO}_3$  surface from high energy intermediates formed during the reaction and block its contact with the aqueous electrolyte. Fabricating such an electrode is attractive due to the simplicity of the synthesis and the earth abundance of the materials used. Because  $\text{WO}_3$  is a binary metal oxide that can be prepared by simple sol-gel processing, we expect few impurities in the synthesis. Using an Earth abundant Fe-based OEC as opposed to more expensive  $\text{IrO}_x$  and Ru-based catalysts also enhances the feasibility of using these electrodes in an actual PEC cell.

We relay a simple sol-gel synthesis coupled with a photoelectrodeposition to yield  $\text{WO}_3\text{-FeOOH}$  electrodes. These techniques were targeted due to the known high performance and the desired reproducibility in the data recorded on the generated films. Electrodes synthesized using these techniques demonstrated a high degree of consistency, which facilitated the collection of three trials for each Faradaic efficiency measurement to establish a reliable average. Through repeated spin coating and annealing at 500 °C, we are able to obtain a thick (ca. 2  $\mu\text{m}$ ) and dense layer of  $\text{WO}_3$ . We have demonstrated that the addition of the FeOOH co-catalyst on the surface of  $\text{WO}_3$  greatly enhances the Faradaic efficiency for

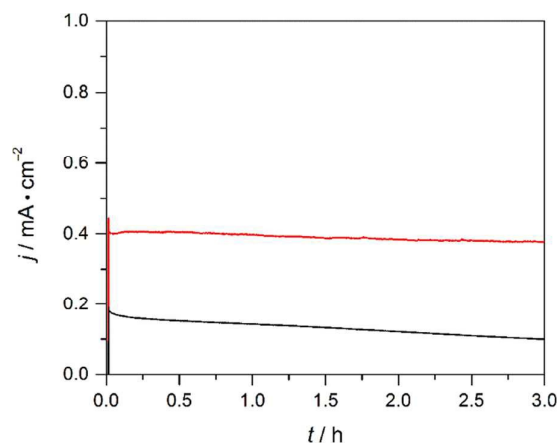
OER as well as its stability in aqueous  $\text{KPi}$  buffers at pH 4 and 7. Our data demonstrate that it may not be necessary to grow a thick co-catalyst layer in order to obtain improved stability and high Faradaic efficiencies for OER. Specifically, cross-sectional SEM imaging does not reveal the formation of a new distinct layer on the surface of  $\text{WO}_3$  after  $\text{FeOOH}$  deposition (Fig. S13, ESI). The  $\text{FeOOH}$  film may be sufficiently thin such that it does not display a contrast difference in the SEM image. Alternatively, the  $\text{FeOOH}$  may deposit in the interstices of the  $\text{WO}_3$  electrode. This result is intriguing since similarly constructed photoanodes

using cobalt phosphate as an OEC have relied on significantly thicker ( $\sim 1 \mu\text{m}$ ) layers to protect the  $\text{WO}_3$  surface.<sup>7</sup> It must be noted that in the previous case, the  $\text{WO}_3$  was grown electrochemically, which yielded very dense films while the sol-gel synthesis presented here produces electrodes of a higher porosity as determined via SEM imaging.

We have observed a marked improvement in electrode stability upon the growth of the  $\text{FeOOH}$  co-catalyst on the surface of  $\text{WO}_3$ . It has been previously reported in the literature that  $\text{H}_2\text{O}_2$  intermediates formed during the course of OER may be responsible for the degradation of the film during the photoelectrolysis of water. To investigate this possibility, we attempted to detect peroxide using a previously reported procedure.<sup>7</sup> In brief a  $\text{WO}_3$  electrode was used in a CPC experiment under 1-sun illumination for 2 hours. A reductive LSV trace in pH 4 0.1 M  $\text{KPi}$  was collected before and after the experiment in an attempt to detect peroxide species adsorbed to the surface (Fig. S14, ESI). We find no detectable peroxide present on the surface of the electrode after CPC under illumination, suggesting that peroxy species in this case may not be the primary cause for the observed degradation of the films. However, because soaking a  $\text{WO}_3$  electrode overnight in a pH 4

$\text{KPi}$  buffer leaves both its morphology and LSV trace unchanged, the observed degradation during electrolysis is likely photochemical in nature. Despite not observing  $\text{H}_2\text{O}_2$ , it is still possible that high energy intermediates such as  $\bullet\text{OH}$  formed during OER may react with  $\text{WO}_3$ .

Although the growth of the  $\text{FeOOH}$  on the sol-gel  $\text{WO}_3$  films does enhance the stability and Faradaic efficiency for OER, we observe that adding  $\text{FeOOH}$  leads to a decrease in the chopped-light photocurrent response. We postulate that this effect may stem from three possibilities. First, it is well known that  $\text{WO}_3$  suffers from poor selectivity for OER in a variety of buffered solutions. Indeed, our results demonstrate that the  $\text{WO}_3$  control films only yielded Faradaic efficiencies of ca.  $26.8 \pm 3.2\%$  in a pH 4  $\text{KPi}$  electrolyte under 2-sun illumination, compared to ca.  $95.9 \pm 1.6\%$  Faradaic efficiency for  $\text{WO}_3$ - $\text{FeOOH}$  electrodes. These experiments indicate that in the case of the  $\text{WO}_3$  control, only about  $\sim 27\%$  of the observed current in the CL-LSV may be derived from OER. Because the saturated photocurrent densities were, on average  $0.8 \text{ mA/cm}^2$ , approximately  $0.22 \text{ mA/cm}^2$  of the observed current may be derived from water oxidation. In contrast, using the  $\sim 96\%$  Faradaic efficiency and  $0.4 \pm 0.1 \text{ mA/cm}^2$  saturated current densities for the  $\text{WO}_3$ - $\text{FeOOH}$  electrodes, it is determined that



approximately  $0.384 \text{ mA/cm}^2$  of current in that case is generated from OER.

Fig. 8 depicts CPC plots for a  $\text{WO}_3$  and a  $\text{WO}_3$ - $\text{FeOOH}$  electrode in which the current density has been corrected for the Faradaic efficiency for OER. These data demonstrate that including the  $\text{FeOOH}$  OEC on  $\text{WO}_3$  is still effectively improving both the rate and selectivity for OER since the current derived from OER is significantly greater. This result is noteworthy because if such an electrode were to be used in a PEC water splitting cell, its efficiency for OER needs to be nearly 100%.<sup>31</sup> We hypothesize that the decrease in the observed photocurrent in the CL-LSVs may be due in part to the  $\text{FeOOH}$  effectively barring side reactions from occurring. Thus although there is an

**Fig. 8:** CPC curves corrected for current derived from OER for  $\text{WO}_3$  (black) and  $\text{WO}_3$ - $\text{FeOOH}$  (red) at 1.23V vs. RHE and 1-sun illumination in pH 4 0.1M  $\text{KPi}$  solution.

observed decrease in photocurrent in the CL-LSVs, the actual Faradaic efficiency and turnover frequency for the desired reaction, i.e. the oxygen evolution reaction, is dramatically improved. It should also be noted that during the course of the oxygen detection experiments, visible bubbling was observed on the  $\text{WO}_3$ - $\text{FeOOH}$  and not the  $\text{WO}_3$  controls, which corroborates the fact that the hybrid electrodes have a higher turnover frequency for OER (Movie S1, ESI). Finally, the total amount of  $\text{O}_2$  generated by the  $\text{WO}_3$ - $\text{FeOOH}$  electrodes was 2 – 3 times greater than the total amount generated by the  $\text{WO}_3$  controls across three trials, which further supports the conclusion that  $\text{FeOOH}$  effectively functions as a co-catalyst for OER.

Second, it may also be possible that the  $\text{FeOOH}$  OEC might effectively reduce the total surface area of the electrode. If the OEC is growing within the interstices of the porous electrode, the total active surface area of the electrode will decrease if the  $\text{FeOOH}$  grows sufficiently thick. We report the current density with respect to planar electrode area, so a reduction in active surface area would also reduce the observed current densities since there would be a lower coverage of catalytically active sites on the surface. To probe this question further, we conducted Cottrell experiments in 0.1 M  $\text{KCl}$  solution in the presence of 6 mM  $\text{K}_3[\text{Fe}(\text{CN})_6]$  following a previously reported procedure.<sup>32</sup> In these experiments, the current decay vs. time

was measured for the reduction of  $[\text{Fe}(\text{CN})_6]^{3-}$  to  $[\text{Fe}(\text{CN})_6]^{4-}$  in solution (Fig. S15, ESI), and we find that the electrochemically active surface area does not change significantly before and after the PEC-EC FeOOH film growth ( $1.06 \text{ cm}^2$  for the  $\text{WO}_3$ -FeOOH versus  $1.07 \text{ cm}^2$  for the  $\text{WO}_3$  electrode). Thus, we conclude that a change in active surface area upon deposition of the FeOOH does not play a significant role in the observed decrease in photo-current density in the CL-LSVs.

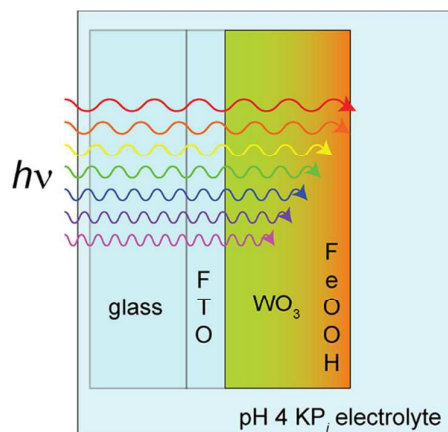
However, a third possibility for the observed decrease in saturated photocurrent may stem from parasitic light absorption from the FeOOH film. Indeed, the Kubelka-Munk  $F(R)$  spectrum of an FeOOH spectrum grown on FTO (Fig S6, ESI) demonstrates that this layer can behave as a strong light absorber, and it may therefore compete with  $\text{WO}_3$  for photon

**Scheme 1.**

absorption. To probe this question further, we plotted the results of the EQE experiments as the ratio of EQE  $\text{WO}_3$ -FeOOH / EQE  $\text{WO}_3$  at each wavelength (Fig. S16 ESI). We observe a decrease in EQE with an increase in wavelength. Because we back illuminated the electrodes during this experiment, photons must first travel through the FTO/ $\text{WO}_3$  interface of the film. Because longer wavelength photons have less energy, they are less likely to be absorbed closest to the FTO/ $\text{WO}_3$  interface. As a result, they travel further through the film and nearer to the  $\text{WO}_3$ /FeOOH junction where they can be parasitically absorbed by the FeOOH OEC, illustrated in Scheme 1. This explains why the ratio of EQE  $\text{WO}_3$ -FeOOH/EQE  $\text{WO}_3$  decreases with increasing wavelength and suggests that parasitic absorption from the FeOOH reduces the number of photons reaching the  $\text{WO}_3$  which in turn decreases the photocurrent response.

Finally, our results indicate that incorporating FeOOH onto  $\text{WO}_3$  appears to decrease the EQE by a maximum of 10% in the region of near UV (350 – 400 nm). We hypothesize that the observed effect may again be related to the difference in Faradaic efficiencies between the two systems as well as competitive light absorption from the FeOOH. EQE simply measures current out regardless of the reaction from which it is generated. Thus, it is possible that  $\text{WO}_3$  may display a higher EQE because it transfers holes to  $\text{H}_2\text{PO}_4^-$ ,  $\text{HPO}_4^{2-}$ , or  $\text{PO}_4^{3-}$  with  $\bullet\text{OH}$  to form peroxodiphosphate ( $\text{P}_2\text{O}_8^{4-}$ ) or peroxophosphate ( $\text{PO}_5^{3-}$ ).<sup>30</sup> Additionally, previous works indicate that  $\text{WO}_3$  will readily oxidize kinetically accessible species in solution.<sup>24,26,33</sup> In stark contrast, our work indicates that  $\text{WO}_3$ -FeOOH electrodes will only transfer holes to water yielding  $\text{O}_2$  as the only product in the same  $\text{KP}_i$  solution. Because OER on FeOOH occurs a lower overpotential, the increase in selectivity could in part explain why adding FeOOH decreases the EQE and saturated photocurrent in CL-LSVs. Additionally, competitive light absorption from the FeOOH layer also plays an important role since the ratio of EQE  $\text{WO}_3$ -FeOOH/EQE  $\text{WO}_3$  decreases with increasing wavelength.

## Conclusions



A simple ion-exchange and spin-coating sol-gel method gives rise to high quality, solar-responsive  $\text{WO}_3$ . Adding the solid-state FeOOH OEC by electrochemical and photoelectrochemical methods increases electrode stability and Faradaic efficiency for PEC OER in 0.1 M  $\text{KP}_i$  buffers. When a bare  $\text{WO}_3$  electrode is used, the Faradaic efficiency for OER at pH 4 is  $26.8 \pm 3.2\%$ , which indicates that a significant portion of the measured current is derived from competing side reactions. Furthermore,  $\text{WO}_3$  electrodes display poor stability at higher pH, which is reflective of photodegradation processes that may occur during the course of OER. In contrast, when a thin FeOOH layer is photoelectrochemically grown on the surface of these  $\text{WO}_3$  electrodes the Faradaic efficiency is dramatically increased up to  $95.9 \pm 1.6\%$ . Furthermore, this OEC significantly improves electrode stability in aqueous solutions up to pH 7. The  $\text{WO}_3$  electrodes used in this study were not optimized to enhance the reaction rate with respect to the active electrode surface area exposed to the electrolyte. Thus, present work focuses on generating nanostructured electrodes to yield a more efficient  $\text{WO}_3$ -FeOOH system.

## Acknowledgements

We would like to thank Mr. Roy Wentz for constructing the custom glass PEC cells used in our work. Additionally, we would like to thank Mr. Derek Fisher from Ocean Optics for assistance with our fluorescence probe as well as Dr. Stephen Maldonado and Ms. Betsy Brown for experimental assistance with the EQE measurements. This research was supported by a grant from the U.S. Department of Energy, DE-SC0006587. J.G.V. was supported by the 2014 University of Michigan NSF-REU program in the Chemical Sciences (CHE-1062654). SEM instrumentation at the University of Michigan Electron Microbeam Analysis Laboratory was funded by NSF Grant DMR-0320710.

## Notes and references

- 1 B. D. Alexander, P. Kulesza, I. Rutkowska, R. Solarska and J. Augustynski, *J. Mater. Chem.*, 2008, **18**, 2298–2303.

Journal Name	ARTICLE
2 K. Maeda, M. Higashi, D. Lu, R. Abe and K. Domen, <i>J. Am. Chem. Soc.</i> , 2010, <b>132</b> , 5858–5868.	21 C. Santato, M. Odziemkowski, M. Ulmann and J. Augustynski, <i>J. Am. Chem. Soc.</i> , 2001, <b>123</b> , 10639–10649.
3 R. Abe, M. Higashi and K. Domen, <i>ChemSusChem</i> , 2011, <b>4</b> , 228–237.	22 R. Solarzka, R. Jurczakowski and J. Augustynski, <i>Nanoscale</i> , 2012, <b>4</b> , 1553.
4 S. S. K. Ma, K. Maeda, R. Abe and K. Domen, <i>Energy Environ. Sci.</i> , 2012, <b>5</b> , 8390.	23 A. Damjanovic, A. Dey and J. O. Bockris, <i>Electrochim. Acta</i> , 1966, <b>11</b> , 791–814.
5 F. Amano, D. Li and B. Ohtani, <i>Chem. Commun. (Camb.)</i> , 2010, <b>46</b> , 2769–2771.	24 J. C. Hill and K. Choi, <i>J. Phys. Chem. C</i> , 2012, <b>116</b> , 7612–7620.
6 G. Wang, Y. Ling, H. Wang, X. Yang, C. Wang, J. Z. Zhang and Y. Li, <i>Energy Environ. Sci.</i> , 2012, <b>5</b> , 6180.	25 C. H. Henry, R. A. Logan and F. R. Merritt, <i>J. Appl. Phys.</i> , 1978, <b>49</b> , 3530.
7 J. A. Seabold and K. Choi, <i>Chem. Mater.</i> , 2011, <b>23</b> , 1105–1112.	26 Q. Mi, A. Zhanaidarova, B. S. Brunshwig, H. B. Gray and N. S. Lewis, <i>Energy Environ. Sci.</i> , 2012, <b>5</b> , 5694.
8 J. E. Yourey and B. M. Bartlett, <i>J. Mater. Chem.</i> , 2011, <b>21</b> , 7651–7660.	27 Q. Mi, R. H. Coridan, B. S. Brunshwig, H. B. Gray and N. S. Lewis, <i>Energy Environ. Sci.</i> , 2013, <b>6</b> , 2646.
9 R. Liu, Y. Lin, L. Y. Chou, S. W. Sheehan, W. He, F. Zhang, H. J. M. Hou and D. Wang, <i>Angew. Chemie - Int. Ed.</i> , 2011, <b>50</b> , 499–502.	28 G. Bardizza, D. Pavanello, H. Mullejans and T. Sample, <i>Prog. Photovoltaics Res. Appl.</i> , 2014, <b>29th EU PV</b> .
10 R. S. Lillard, G. S. Kanner and D. P. Butt, <i>J. Electrochem. Soc.</i> , 1998, <b>145</b> , 2718.	29 J. W. Schultze, S. Mohr and M. M. Lohrengel, <i>J. Electroanal. Chem.</i> , 1983, <b>154</b> , 57–68.
11 J. Augustynski, R. Solarzka, H. Hagemann and C. Santato, <i>Proc. SPIE</i> , 2006, <b>6340</b> , 63400J–63400J–9.	30 M. E. G. Lyons and L. D. Burke, <i>J. Electroanal. Chem. Interfacial Electrochem.</i> , 1984, <b>170</b> , 377–381.
12 J. a Seabold and K.-S. Choi, <i>J. Am. Chem. Soc.</i> , 2012, <b>134</b> , 2186–92.	31 M. Grätzel, <i>Nature</i> , 2001, <b>414</b> , 338–344.
13 M. W. Louie and A. T. Bell, <i>J. Am. Chem. Soc.</i> , 2013, <b>135</b> , 12329–12337.	32 S. J. Konopka and B. McDuffie, <i>Anal. Chem.</i> , 1970, <b>42</b> , 1741–1746.
14 S. Klaus, Y. Cai, M. W. Louie, L. Trotochaud and A. T. Bell, <i>J. Phys. Chem. C</i> , 2015, 150303215355006.	33 Q. Mi, R. H. Coridan, B. S. Brunshwig, H. B. Gray and N. S. Lewis, <i>Energy Environ. Sci.</i> , 2013, <b>6</b> , 2646.
15 L. Trotochaud, S. L. Young, J. K. Ranney and S. W. Boettcher, <i>J. Am. Chem. Soc.</i> , 2014, <b>136</b> , 6744–6753.	
16 D. K. Bediako, Y. Surendranath and D. G. Nocera, <i>J. Am. Chem. Soc.</i> , 2013, <b>135</b> , 3662–3674.	
17 W. D. Chemelewski, J. R. Rosenstock and C. B. Mullins, <i>J. Mater. Chem. A</i> , 2014, <b>2</b> , 14957.	
18 W. D. Chemelewski, H. C. Lee, J. F. Lin, A. J. Bard and C. B. Mullins, <i>J. Am. Chem. Soc.</i> , 2014.	
19 A. G. Tamirat, W.-N. Su, A. A. Dubale, H.-M. Chen and B.-J. Hwang, <i>J. Mater. Chem. A</i> , 2015, <b>3</b> , 5949–5961.	
20 K. J. McDonald and K.-S. Choi, <i>Energy Environ. Sci.</i> , 2012, <b>5</b> , 8553–8557.	